Section 4.4: Continuous or Time Integrated PM Results and Summary

W. Patrick Arnott, John Walker, Eric Fujita, Dave Campbell, and Sebastian Upallalli
Desert Research Institute
Reno NV

Abstract

Emission rates for gasoline powered vehicles were determined by the dynamometer evaluation method where vehicles are driven through prescribed cycles on rollers that provide electrodynamic resistance that simulates road drag. The unified cycle was used where the first two phase in cold start is repeated again after warm start following a 'hot soak' of 8 minutes. Black carbon emission rates are determined by calculation from data obtained in real time aerosol light absorption measurements accomplished using the DRI photoacoustic instrument. Optical particle mass was obtained with two nephelometers, the Thermo Electron Corporation DataRam4 and the TSI DustTrak.

Specific findings are as follows. Photoacoustic measurements of black-carbon mass concentration has sufficient time response and dynamic range for use on a range of vehicles from relatively clean to relatively dirty vehicles evaluated on dynamometers. All vehicles tested, including late model spark ignition vehicles, had black carbon emission. Cold start black carbon and PM emission rates can be two to eight times larger than warm start emission rates. Relatively clean spark ignition vehicles have black carbon emissions that generally follow the more aggressive portions of the driving cycle, with maximum emissions typical during cold start and a secondary peak during aggressive acceleration. By contrast, older vehicles emitted a large amount of black carbon during the entire driving cycle. DustTrak nephelometer measurements of PM were in the range of filter-based measurements. DataRam4 PM measurements were in accord with DustTrak values for vehicles with lower emission rates, though were far in excess of both the DustTrak and the filter-based measurements for vehicles with high emission rates.

Examples are given in this section of the stratum averaged real time response of vehicles to dynamometer speed. Time averaged continuous PM from the nephelometers is compared with gravimetric measurements obtained with the Teflon filters. BC and PM emission rates are presented from time averages of the continuous data.

INTRODUCTION

Motor vehicle manufactures have a long history of interest in measurement of black carbon emissions from vehicles with use of the photoacoustic method (Roessler 1984). A more recent study evaluated methods for continuous measurement of PM from light duty diesel vehicles tested on a dynamometer (Moosmüller, Arnott et al. 2001; Moosmüller, Arnott et al. 2001). The key findings of this work were that the time-averaged tapered-element oscillating microbalance (TEOM) data showed close correlation with PM2.5 measurements using Teflon

filters. The TEOM had considerably more noise than the DustTrak nephelometer also used for PM2.5 measurement, though the DustTrak showed variable correlation with Teflon filter mass with the key dependence related to the amount of organic carbon in the exhaust and very likely, the change in particle size with vehicle model year. Photoacoustic (PA) measurements of black carbon (BC) were found to correlate well with elemental carbon measurements accomplished thermal optical reflectance analysis using the IMPROVE protocol (Chow, Watson et al. 1993) (TOR-IMPROVE) for the definitions of the various organic carbon (OC) and elemental carbon (EC) stages as well as the correction for optical pyrolysis. An efficiency factor was obtained for converting aerosol light absorption measurements by the photoacoustic method to BC such that for light duty diesel vehicles, BC = EC. The instrument suite of TSI DustTrak and Thermo Electron Corporation DataRam4 nephelometers for total PM, and DRI photoacoustic instrument for black carbon mass concentration were deployed during the study reported on here. DRI also was responsible for operation of the quartz crystal microbalance, though responsibility for final data analysis and reduction lies with the EPA.

MEASUREMENT METHODS

The real-time methods used to measure PM included the Quartz Crystal Microbalance (QCM) manufactured by Sensors Inc, the DustTrack nephelometer manufactured by TSI, and the Mie DataRam4 manufactured by Thermo Electron Inc. Real time black carbon mass concentration measurements were obtained using a photoacoustic instruments operating at 1047 nm, and this instrument was manufactured by the Desert Research Institute (Arnott, Zielinska et al. 2004). This same instrument suite was previously evaluated in measurements of emissions from light duty diesel trucks on a dynamometer (Moosmüller, Arnott et al. 2001; Moosmüller, Arnott et al. 2001). In brief, the findings of this previous work were derived from the

comparison of traditional filter samples of PM and EC with time averages obtained from these real-time instruments. The DustTrak, being an optical measurement method, had sensitivity to both particle composition and size. Photoacoustic measurements of BC agreed quite favorably with EC measurements obtained from the Improve Protocol Thermal Optical Reflectance (TOR) measurement obtained from samples collected on quartz filters. TOR analysis is described in (Chow, Watson et al. 1993). With 1 second time constants the precision of the DustTrak and photoacoustic instrument are 1 μg m^{-3}.

Nephelometer Measurements of Aerosol Light Scattering and Relation to Particle Mass

Nephelometers are designed to measure the light scattered by particles. While these instruments in general have performance issues associated with angular truncation and non-ideality in the detectors (Anderson and Ogren 1998), the angular response of the nephelometers used in this study have not been reported in the literature.

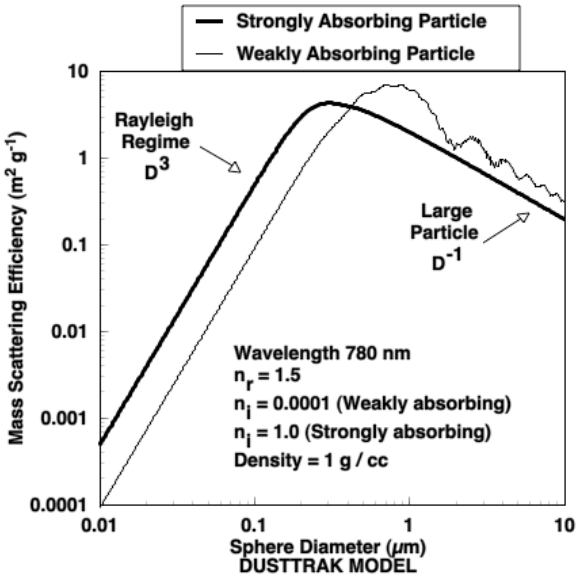

Figure 1. Theoretical mass scattering efficiency for a perfect nephelometer. Strongly absorbing particles such as black carbon are given by the thick curve and weakly absorbing particles such as organic carbon are given by the other curve.

Figure 1 indicates the mass-weighted scattering efficiency as a function of particle size for a wavelength of 760 nm, pertinent to the DustTrak nephelometer. Note that if the DustTrak were a perfect instrument for measuring particle mass the mass scattering efficiency curve would be a constant value and there would be no composition dependence. The DustTrak mass calibration factor is determined by the manufacturer using an ISO standard Arizona Road Dust having particle size distribution peak near 2 microns. However, typical combustion particles have mass weighted sizes near 0.3 microns, but because this size is about at the same value of mass scattering efficiency as the Arizona road dust value, and to the left of the peak of the curve shown in Fig. 1, the DustTrak produces mass concentrations in the ball park of the correct value. It should be noted that nephelometers are very sensitive to particles of sizes larger than about 0.1 to 0.3 microns, depending on composition, but that their calibration as a mass standard is dependent especially on particle size as well as composition to a lesser extent (Sioutas, Kim et al. 2000).

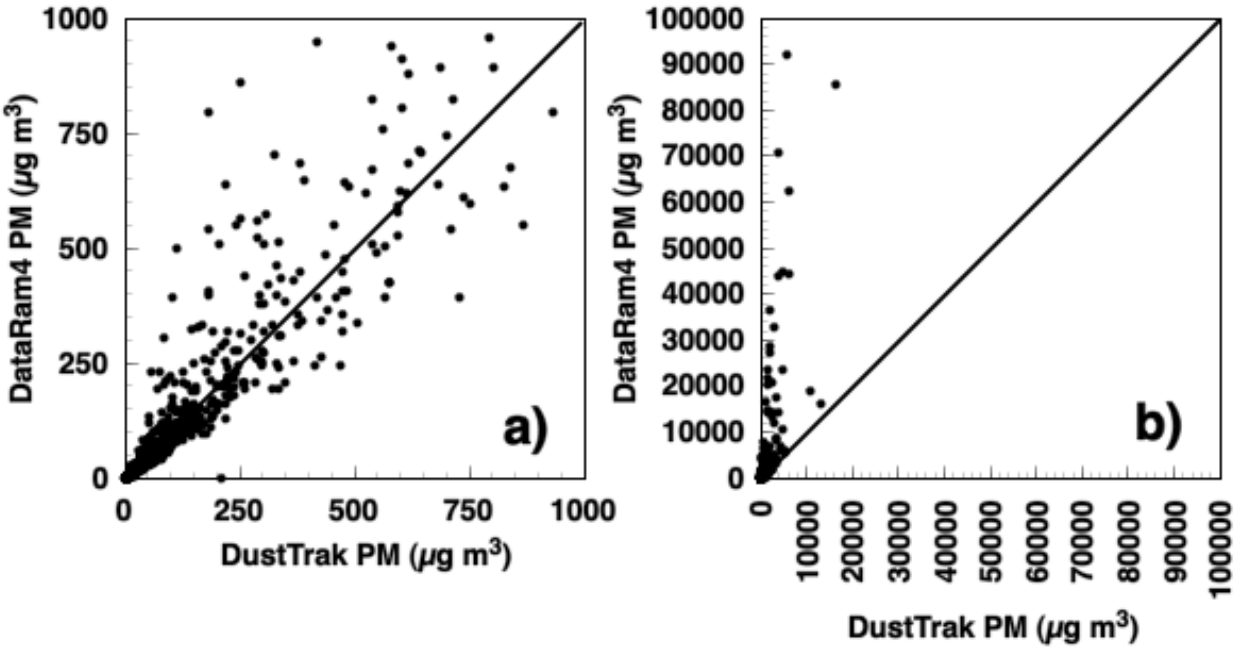

Figure 2. PM data from the DustTrak and DataRAM4 for a) low and b) high range.

The Mie DataRAM4 (DR) manufactured by Thermo Electron Inc is a more sophisticated instrument than the TSI DustTrak (DT). The DR measures light scattering at two wavelengths such as 880 nm and 760 nm. Why is this done? Because use of two wavelengths allows for better knowledge of particle size as it relates to the mass scattering efficiency factor shown in Fig. 1. The curves in Fig. 1 were computed for a wavelength of 760 nm. If they were computed for a wavelength of 880 nm the peak in the curves would be shifted to the right, so that for combustion size particles the 880 nm scattering amount would be less than the 760 nm amount. The ratio of these two values would give a measure of particle size.

Figure 2 shows scatter plots of time averaged DustTrak and Mie DataRAM4 phase averaged data (i.e. each point represents a time average from phase 1, 2, or 3 of the unified cycle). Note that for mass concentrations below 250 ug m^{-3} relative agreement is found among these instruments as illustrated in Fig. 2a. However much more scatter occurs for high mass concentrations as shown in Fig. 2a. Finally, Fig. 2b shows that the DataRAM4 values are much in excess of those of the DustTrak. The DataRAM4 manufacturer states an upper range for the instrument of 400,000 ug m^{-3}, though a recent email correspondence with an expert (Wayne Harmon) on the instrument from the company that manufactures it is quoted here: "For vehicles with high emission, it may be necessary to dilute the air sample. The background will become slightly elevated due to contamination if high concentrations (above 20 mg/m3) are sampled for an hour or more." Notice that 20 mg/m3 is 20,000 ug m^{-3}, well below the stated upper range of the instrument.

Which nephelometer is closer to the "actual value" of aerosol -mass concentration? To answer this question one needs to keep in mind that aerosol mass concentration is a fleeting quantity. Change the air temperature or gaseous composition and the gas to particle phase

partition is upset. Capture particles on filters and gases may also adsorb onto the particles and filters.

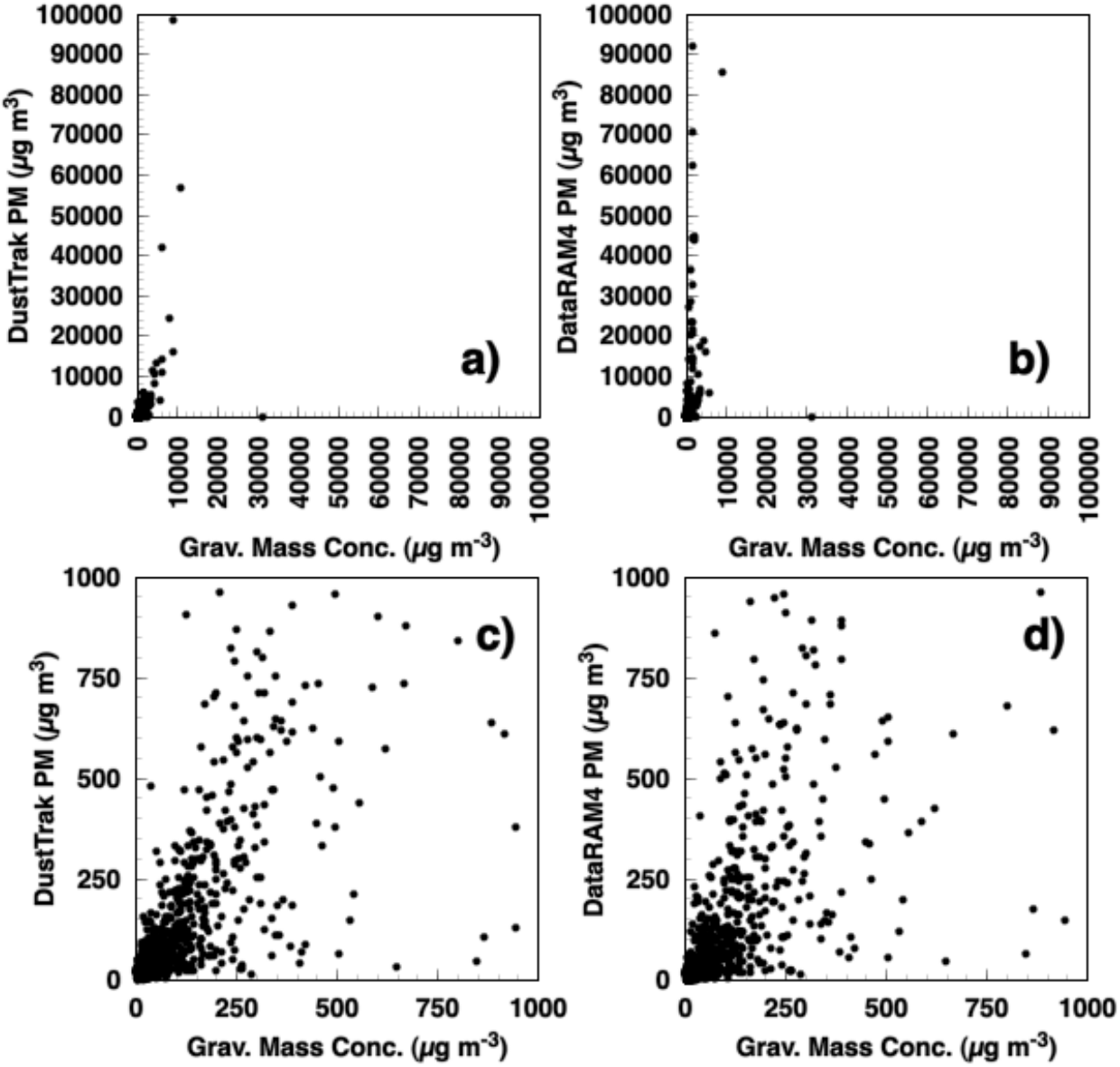

Figure 3. Scatter plots of gravimetric mass and nephelometer mass for the DustTrak and DataRAM4 over a wide range in a) and b) and a narrower range in c) and d).

Figure 3 shows the comparison of gravimetric mass with nephelometer mass for phase averaged data. Note in Figs. 3a) and 3b) that both nephelometers produce values much larger than gravimetric mass for very high values of mass, though that the DustTrak is closer to

gravimetric mass than is the DataRAM4. Over the reduced range shown in Figs 3c) and 3d) much scatter is noted between nephelometer mass and gravimetric mass, and that the DT and DR have about the same amount of scatter. It is likely that variations in particle size and composition, and uncertainty in gravimetric mass give rise to the scattering seen in Fig. 3.

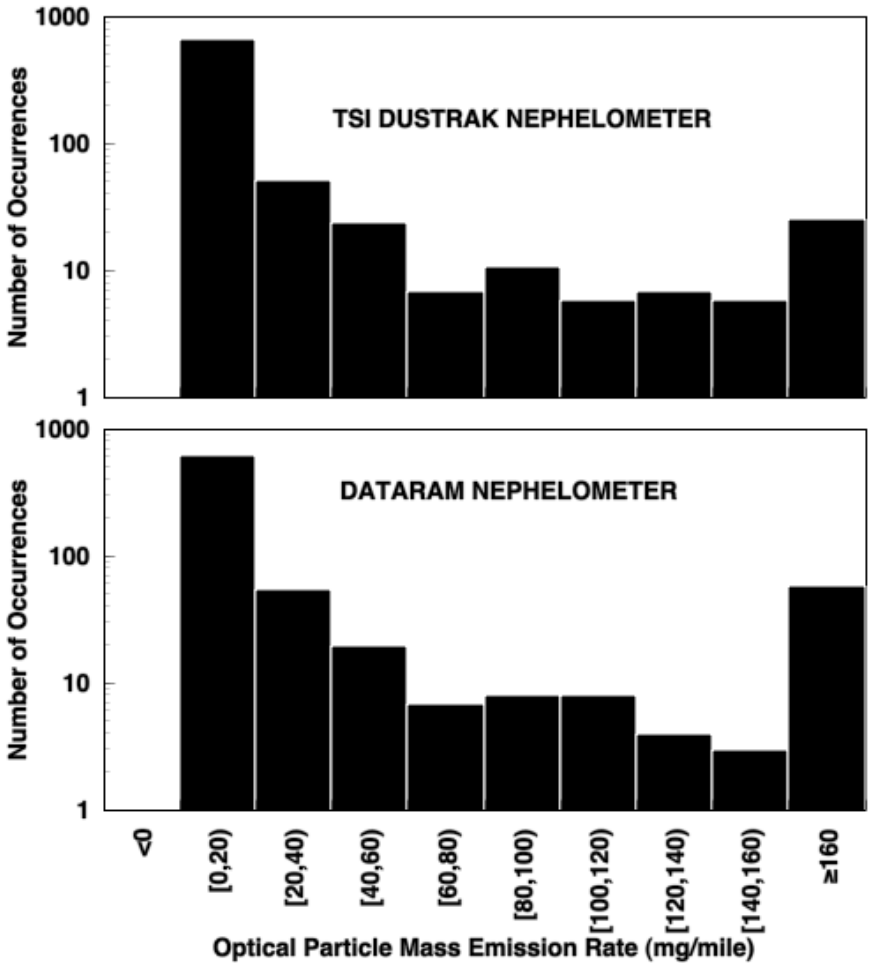

Figure 4. Histograms of nephelometer PM emission rates for the DT and DR.

Figure 4 shows histograms of emission rates computed from DustTrak and DataRAM4 nephelometer measurements of PM averaged over phases 1 through 3 of the unified cycle. It was necessary to use a logarithmic plot because the emission rates in the smallest bin, 0-20 mg/mile, dominate all other measurements. Note that the DataRAM4 indicates considerably

more instances of very large emission rates than does the DustTrak. The gross shape of the distributions are similar.

Photoacoustic Measurements of Aerosol Light Absorption and the Definition of Black Carbon

Photoacoustic instruments have been used in source sampling of black carbon aerosol. Sample air is pulled continuously through an acoustical resonator and is illuminated by laser light that is periodically modulated at the acoustical resonance frequency. Light absorption is manifested in particle heating and this heat transfers rapidly to the surrounding air, inducing pressure fluctuations that are picked up with a microphone on the resonator. Microphones have a very large dynamic range (at least 6 orders of magnitude), so black carbon measurements can be made over a large dynamic range with these instruments. The advancement that has been very important for the continued success of these instruments is the ability to measure very low levels of light absorption. Aerosol light absorption at visible and near IR wavelengths occurs throughout the entire particle volume for typically submicron combustion particles, so black carbon aerosol mass concentration is found to vary in direct proportion with light absorption. Vehicle manufactures pursued these methods in the 1970's and 1980's using bulky Argon Ion lasers and dye lasers (Terhune and Anderson 1977; Japar and Killinger 1979; Japar and Szkarlat 1981; Japar and Szkarlat 1981; Japar, Szkarlat et al. 1984; Roessler 1984), and a resurgence of interest has emerged in research laboratories that coincides with technological developments in compact, efficient laser sources (Petzold and Niessner 1994; Petzold and Niessner 1995; Arnott, Moosmüller et al. 1999; Moosmüller, Arnott et al. 2001).

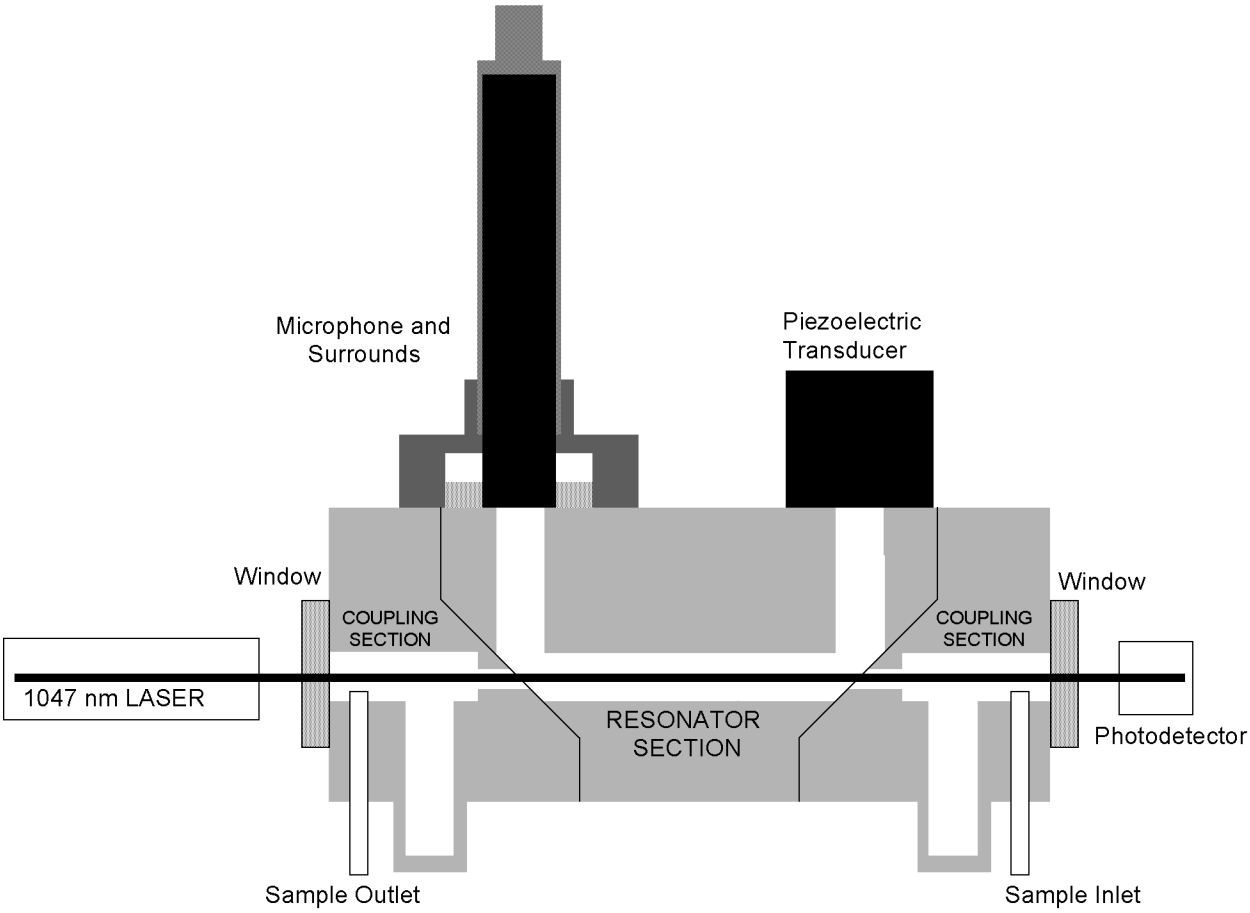

Figure 5. Schematic of the photoacoustic instrument.

The photoacoustic instrument developed for this work operates at a convenient wavelength of 1047 nm where gaseous interference is not a problem and where a laser source is available that allows for direct electronic modulation of the power at the resonator frequency.

The acoustical resonator, shown schematically in Fig. 5, was designed for compactness, ease of reproducibility in manufacture, and robustness with respect to use of the instrument in very noisy, dirty sampling environments (Arnott, Moosmueller et al. 2003). The instrument comprises two identical coupling sections, and a third resonator section. These parts are manufactured out of aluminum. The coupling sections allow the laser beam to enter the instrument through windows well separated from the resonator section. The sample inlets and outlets are followed by cavities that are tuned to reduce the coupling of noise into the resonator

section. The resonator section has a horizontal tube that is 1/2 of an acoustic wavelength long, and two vertical tubes that are 1/4 of an acoustic wavelength long. In previous designs (Arnott, Moosmüller et al. 1999), the vertical tubes were at an angle of 45 degrees to the horizontal instead of 90 degrees as they are now, and the tubes were formed from pipe rather than machined with precision. The 90 degrees angles allow for symmetry when deciding where the holes in the resonator are placed to allow for laser beam and sample air passage. The piezoelectric transducer is used as a sound source to occasionally scan the resonator resonance frequency and quality factor for use in calibrating the instrument from an acoustical perspective. The microphone and piezoelectric transducer sit at pressure antinodes of the acoustic standing wave, and the holes in the resonator are at pressure nodes. The instrument is bolted together in three parts for easy disassembly in case it needs to be cleaned. The laser beam passes through the windows and the holes in the resonator section. The laser beam pumps the acoustic wave through light absorption, and the transfer of the associated heat to the surrounding air, in the resonator section.

The photoacoustic instrument measures the aerosol light absorption coefficient (Arnott, Moosmüller et al. 1999; Arnott, Moosmüller et al. 2000), and then a quantity defined as black carbon (BC) is computed from the absorption coefficient. The 'elemental' carbon (EC) part of the exhaust absorbs light at 1047 nm much more strongly than any other common particulate aerosol in exhaust and in the atmosphere so that it is reasonable to associate elemental carbon with aerosol light absorption. Why is it reasonable to associate aerosol light absorption with a black carbon mass concentration (BC)? Because aerosol light absorption occurs throughout the entire particle volume for sufficiently small particles and large wavelengths of light, giving rise to a direct proportionality between the absorption measurement and the aerosol mass for typical

combustion particle of typical size, and for the 1047 nm wavelength used in the instrument. It is perhaps inevitable to speculate that the aerosol complex refractive index could vary with combustion source ((Dalzell and Sarofim 1969) (Fuller, Malm et al. 1999), so that the black carbon measured values could be different for particles actually having the same numbers of carbon atoms in them. And it is possible to postulate that aerosol coatings or adsorbents, or particle morphology, could also give rise to different absorption coefficients than one would observe for uncoated particles. Experiences to date have shown that for an emission source such as a late model diesel that is rich in EC, the Improve protocol method of quantifying EC (Chow, Watson et al. 1993) correlates well with the aerosol light absorption measurement at 1047 nm.

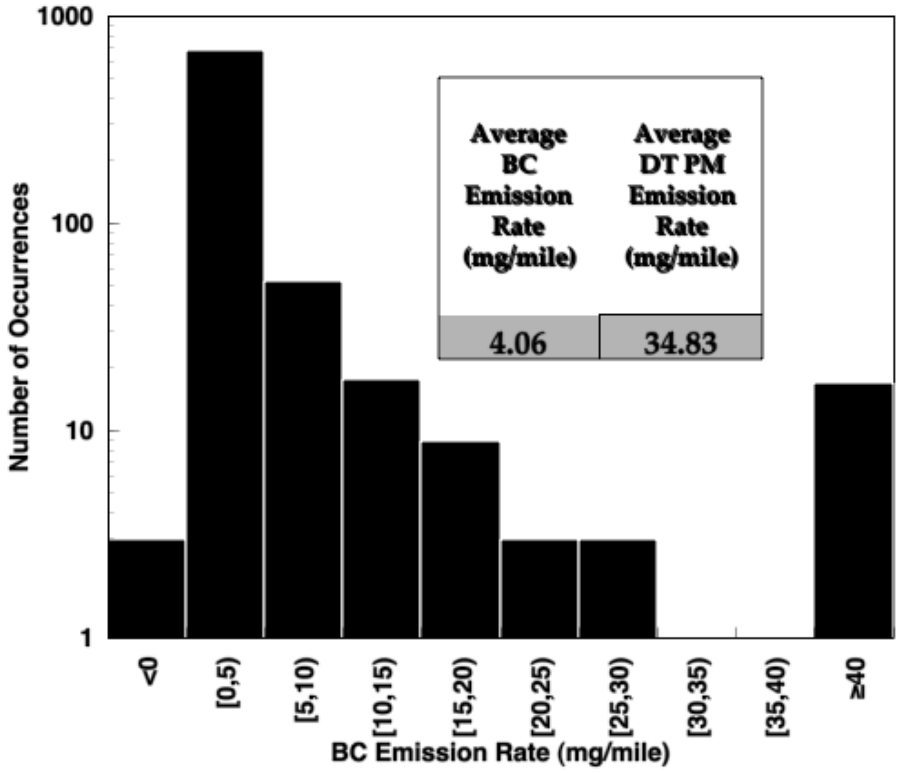

Figure 6. Histogram of BC emission rate, and average emission rate for BC and DT PM, inset.

The following relationship is used to obtain black carbon concentration from the aerosol light absorption measurement at 1047 nm:

$$BC\ (\mu g\ m^{-3}) = 5\ (m^2\ g^{-1})\ B_{abs}\ (Mm^{-1})\ \{measured\ at\ 1047\ nm\}\ . \quad (1)$$

This relationship represents diesel emissions. EC from diesels provide a relatively unambiguous measurement from the various protocols and methods that have been developed though ambient and wood smoke samples have substantial differences (Watson, Chow et al. 1994; Chow, Watson et al. 2001).

Figure 6 shows a histogram of the number of occurrences of different BC emission rates. It has a form similar to the DT and DR emission rate histograms shown in Fig. 4. The average BC emission rate was 4 mg/mile, and the average PM emission rate computed from the DustTrak data was 34 mg/mile. If all of the DustTrak PM is considered to be carbonaceous, then the ratio of BC to PM is around 1/9.

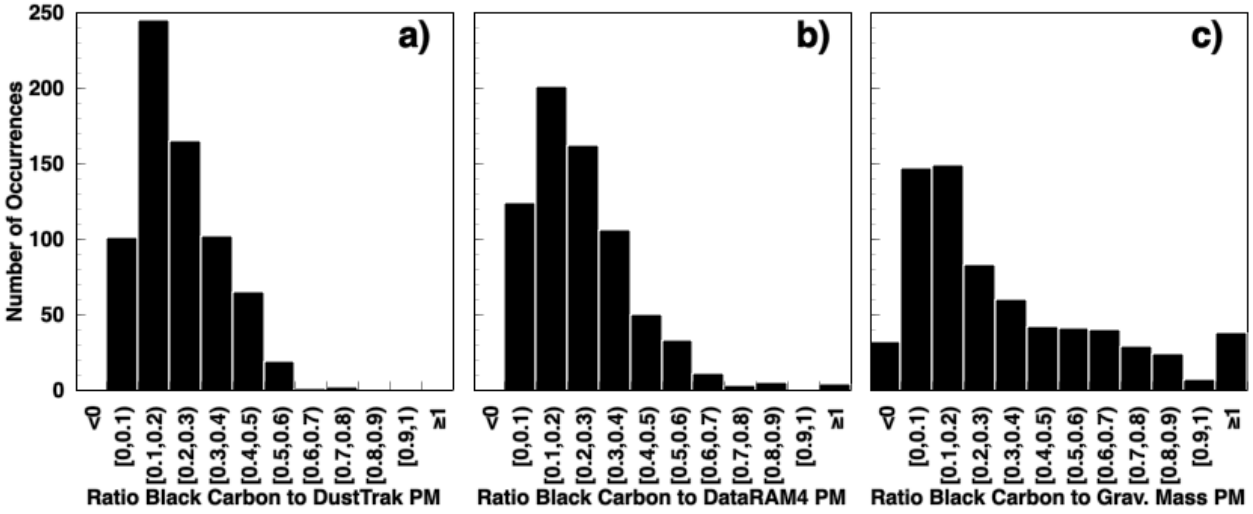

Figure 7. Histograms of the ratio BC to total PM, with total PM from the DustTrak in a), from the DataRAM4 in b), and from the gravimetric mass in c). The vertical scale is the same in each plot. Histograms were developed from phase averaged data, excluding cases where the BC average is less than 2 μg m^{-3}.

Figure 7 shows histograms of the ratio of BC to PM, with PM obtained from the DT and DR nephelometers, and with gravimetric mass. Fig. 7a is the most reasonable representation of this ratio. Most spark ignition PM is known to be organic carbon (OC) and most PM is

associated with total carbon (TC=OC+BC). The DataRAM4 produces too many large values of this ratio as shown in Fig 7b. The gravimetric mass in Fig. 7c when used to compute the ratio BC to PM has a very broad unrealistic histogram, with many values greater than unity, and some less than zero. The uncertainty in the gravimetric mass is much greater than that of all the other PM measures.

Average BC and PM concentrations in each stratum as related to vehicle speed

The utility of continuous measurements of BC and PM are most evident in evaluating the driving conditions that give rise to the bulk of the emissions. Figure 8 through Fig. 15 illustrate the emissions of BC as measured by the photoacoustic instrument, and PM as measured by the DustTrak nephelometer as a function of time. The vehicle speed profile is also overlain on these plots, and this trace is inverted so that the emissions can readily be seen. The captions document the data in detail, though some highlights are given here. Figure 8 is typical of the comparison of phases 1 and 3 of the unified cycle. Phase 1 commences after a cold start of the vehicle, and phase 3 after a warm start. The vehicle speed profile is the same for these phases. Phase 1 emission rates are generally higher than those of phase 3 for all classes of vehicles, though the older vehicles have more emissions at all times. Phase 1 emissions from newer vehicles are associated with accelerations, decelerations, as well as higher speed driving, whereas phase 3 emissions from newer vehicles are mostly closely associated with accelerations. Phase 2 emissions from both cars (Fig. 10) and trucks (Fig. 11) are dominant during the high acceleration portion of the driving cycle before time 900 seconds. To produce the data shown in Figs. 8-15, all data was aligned in time to the start of the unified cycle, and interpolated to 1 second steps.

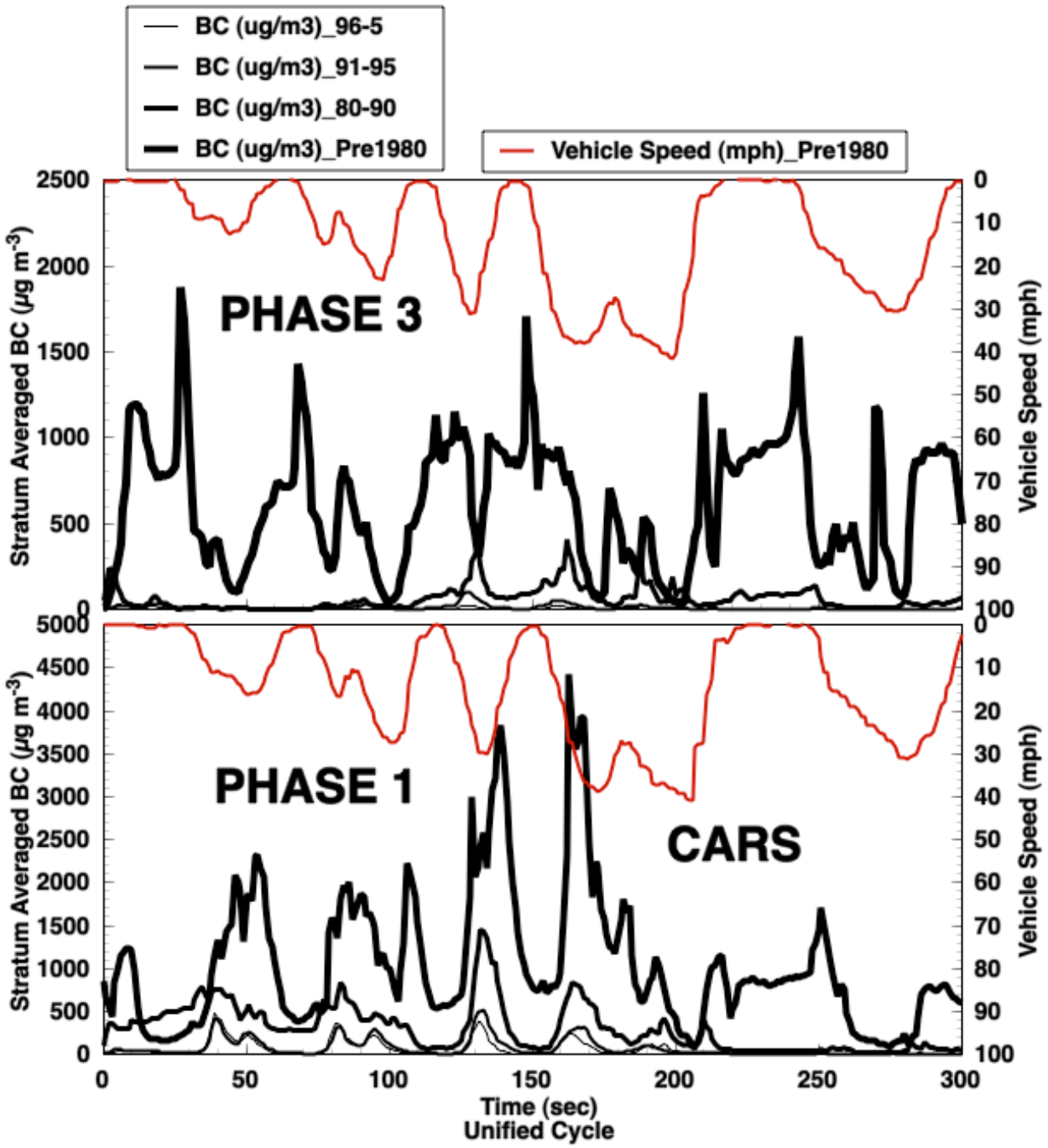

Figure 8. Stratum averaged BC emission for passenger cars as it relates to vehicle speed. Phase 1 follows is associated with a cold start of the vehicles, and phase 3 is an identical driving cycle but one that follows a warm start after an 8 minute soak period. Note that newer cars have much less emission in phase 3.

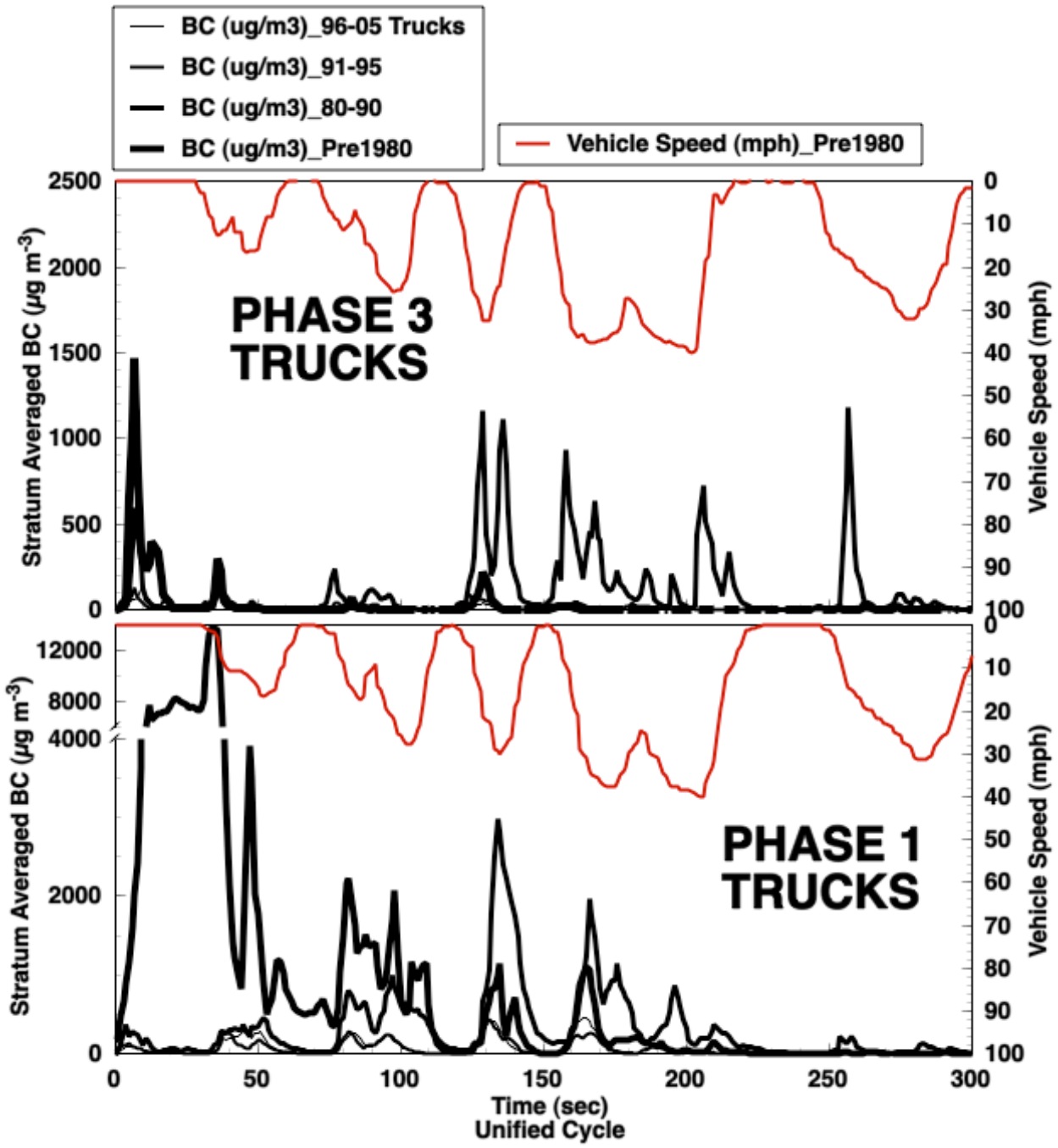

Figure 9. Same as Figure 8, though for trucks rather than cars. Note the high emissions during phase 1 of the oldest truck, and that it is much less in phase 3, illustrating that the warm vehicle emission rates are much lower. Note that there were only 2 trucks in that category. Cleaner trucks behave as cleaner cars.

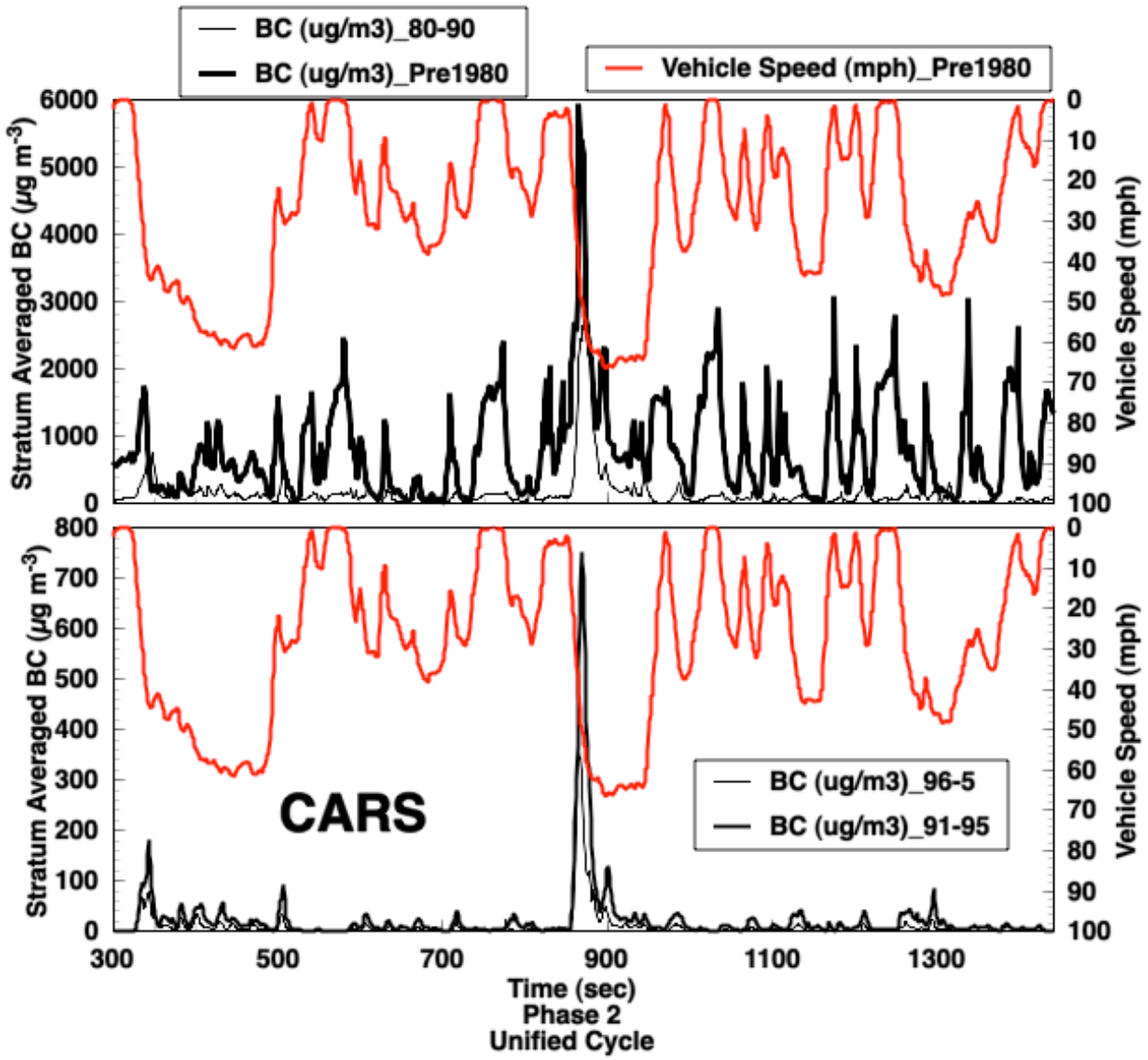

Figure 10. BC emissions during phase 2 of the unified cycle for newer (lower graph) and older (upper graph) vehicles. Note that BC emissions peak during the aggressive acceleration in about the middle portion of the cycle right before 900 seconds. Note in the upper graph that the oldest category of vehicles had high emission on both accelerations as well as decelerations.

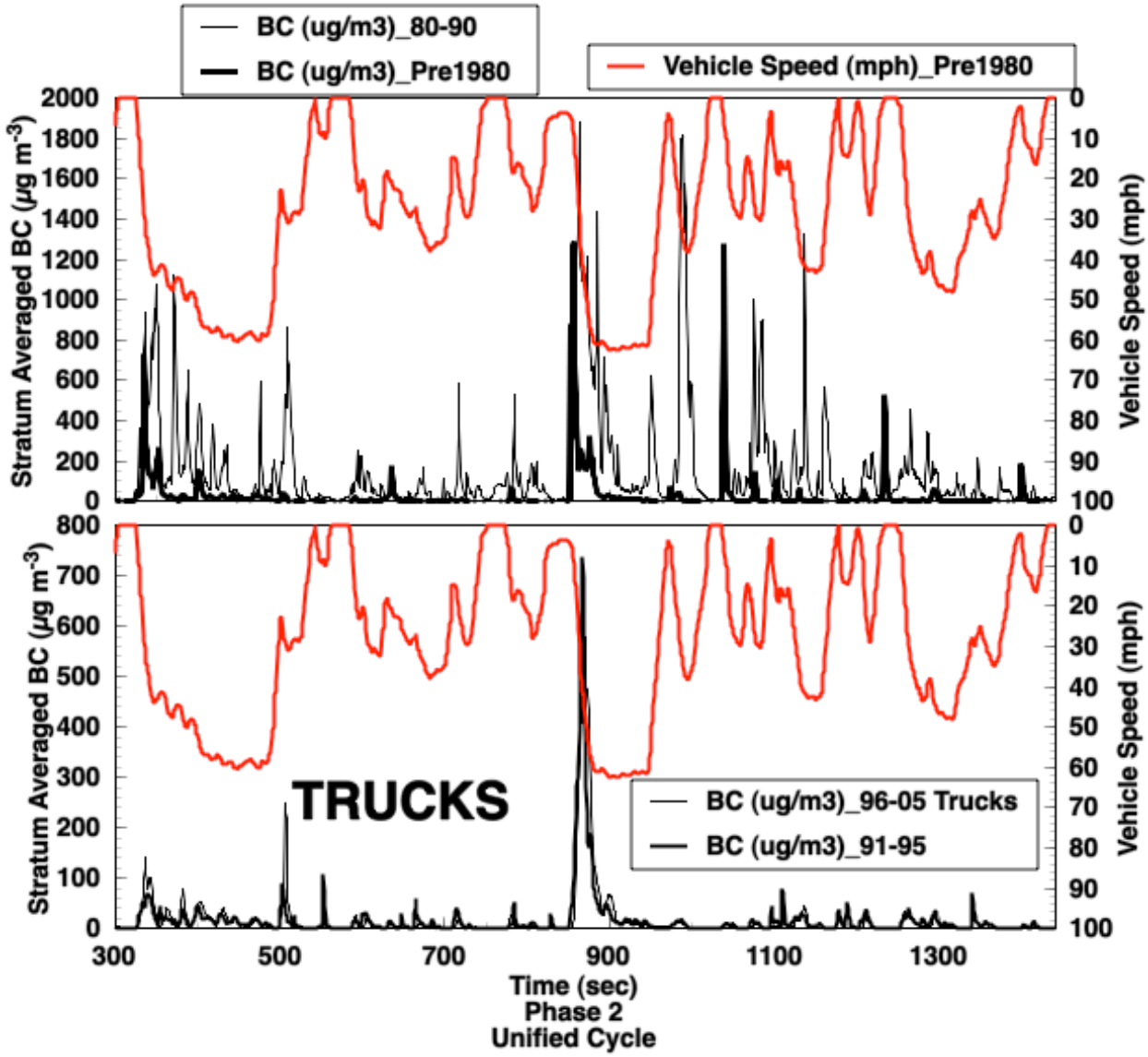

Figure 11. Same as Figure 10, though for trucks instead of cars. Note that in comparing the older cars and trucks that the older trucks had less emission during phase 2 than did the cars. This could be an artifact of the sample size, though it does point out that older vehicles, when warmed up, can have modest emission rates.

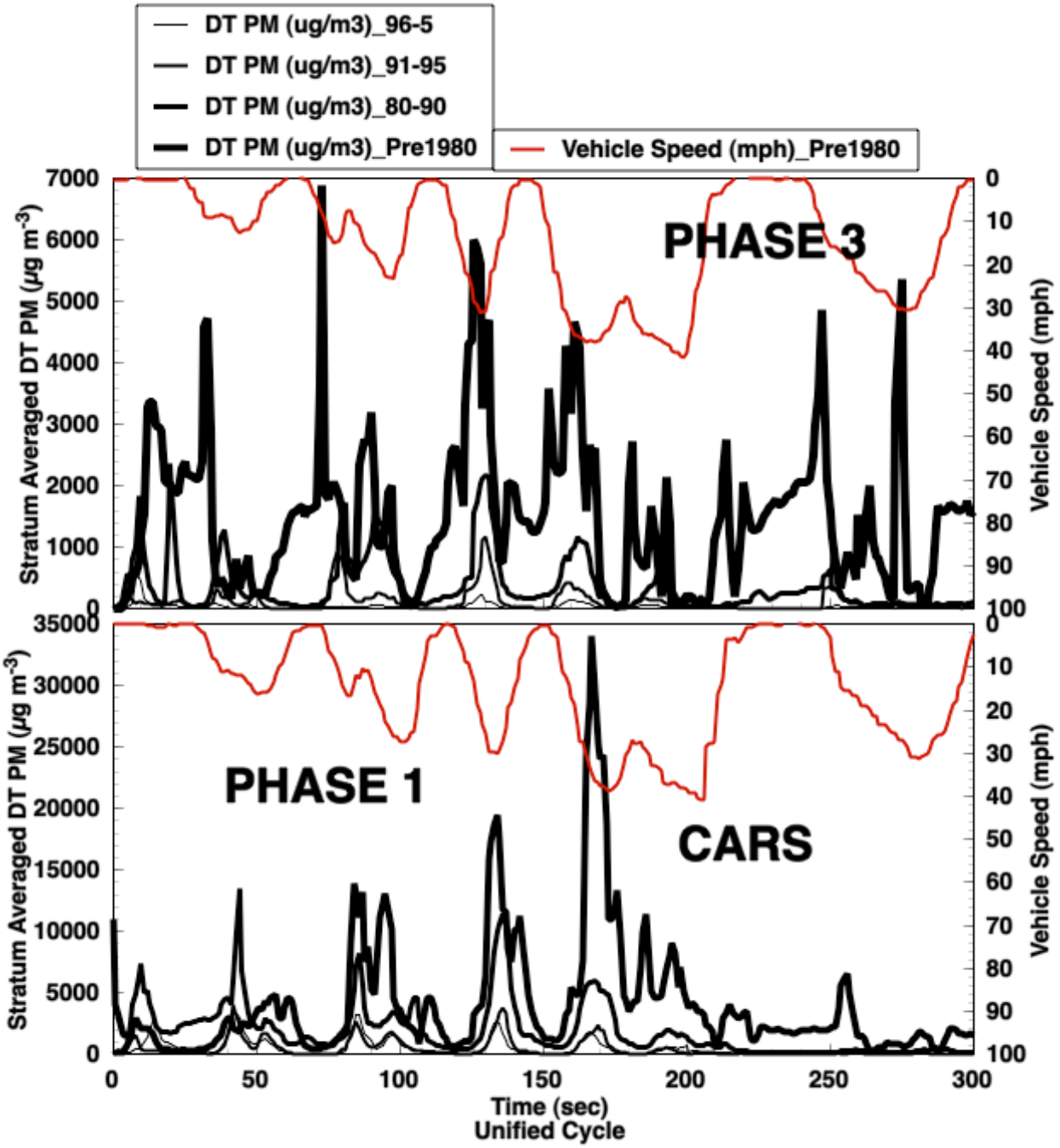

Figure 12. Stratum averaged DustTrak PM emission for passenger cars as it relates to vehicle speed. Phase 1 follows is associated with a cold start of the vehicles, and phase 3 is an identical driving cycle but one that follows a warm start after an 8 minute soak period. Note that newer cars have much less emission in phase 3.

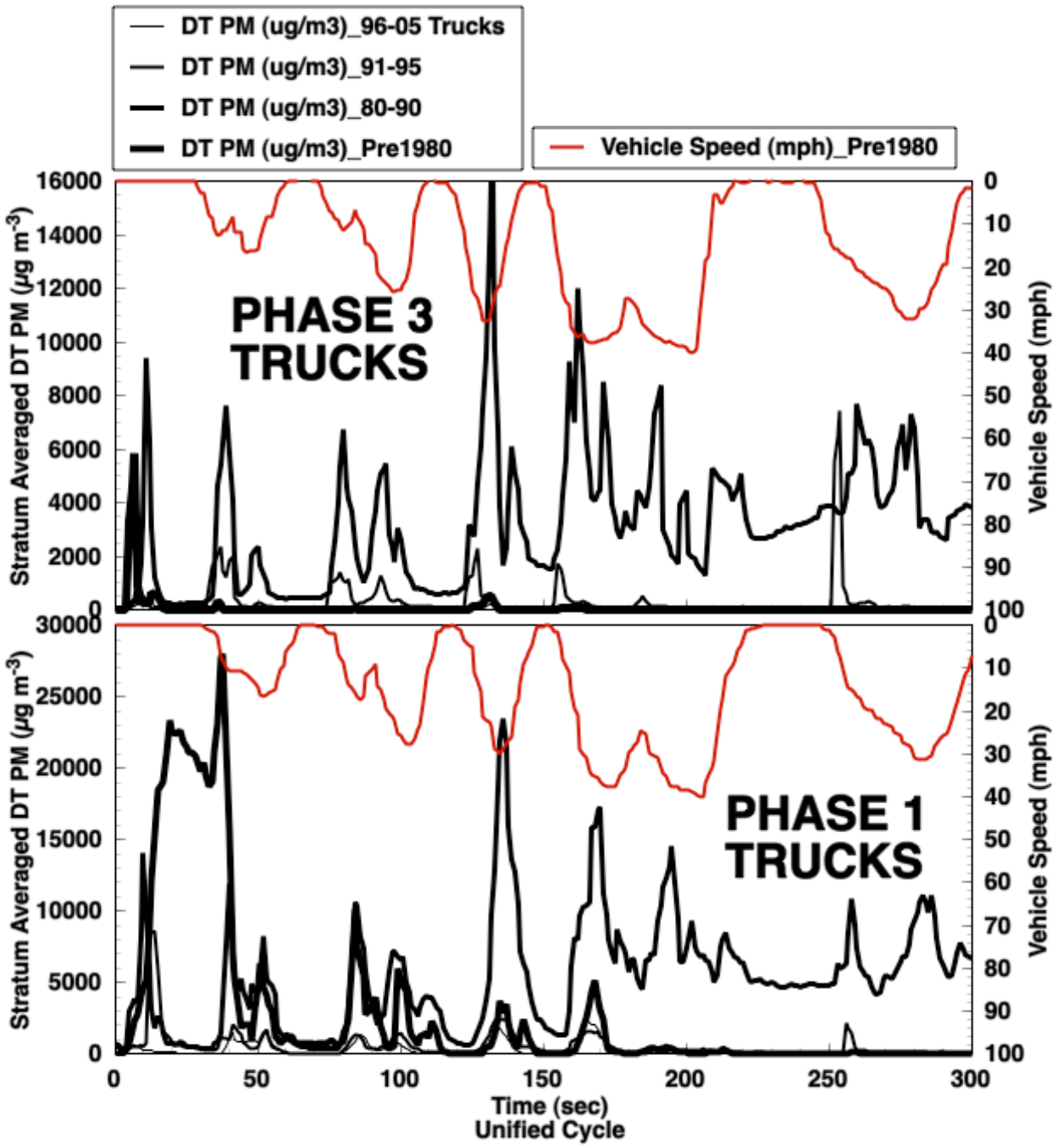

Figure 13. Same as Figure 12, though for trucks rather than cars. Note the high emissions during phase 1 of the oldest truck, and that it is much less in phase 3, illustrating that the warm vehicle emission rates are much lower. Note that there were only 2 trucks in that category. Cleaner trucks behave as cleaner cars. Note that PM emission rates of the model year 80-90 vehicles during phase 3 are high and seem to have little relation with the driving cycle.

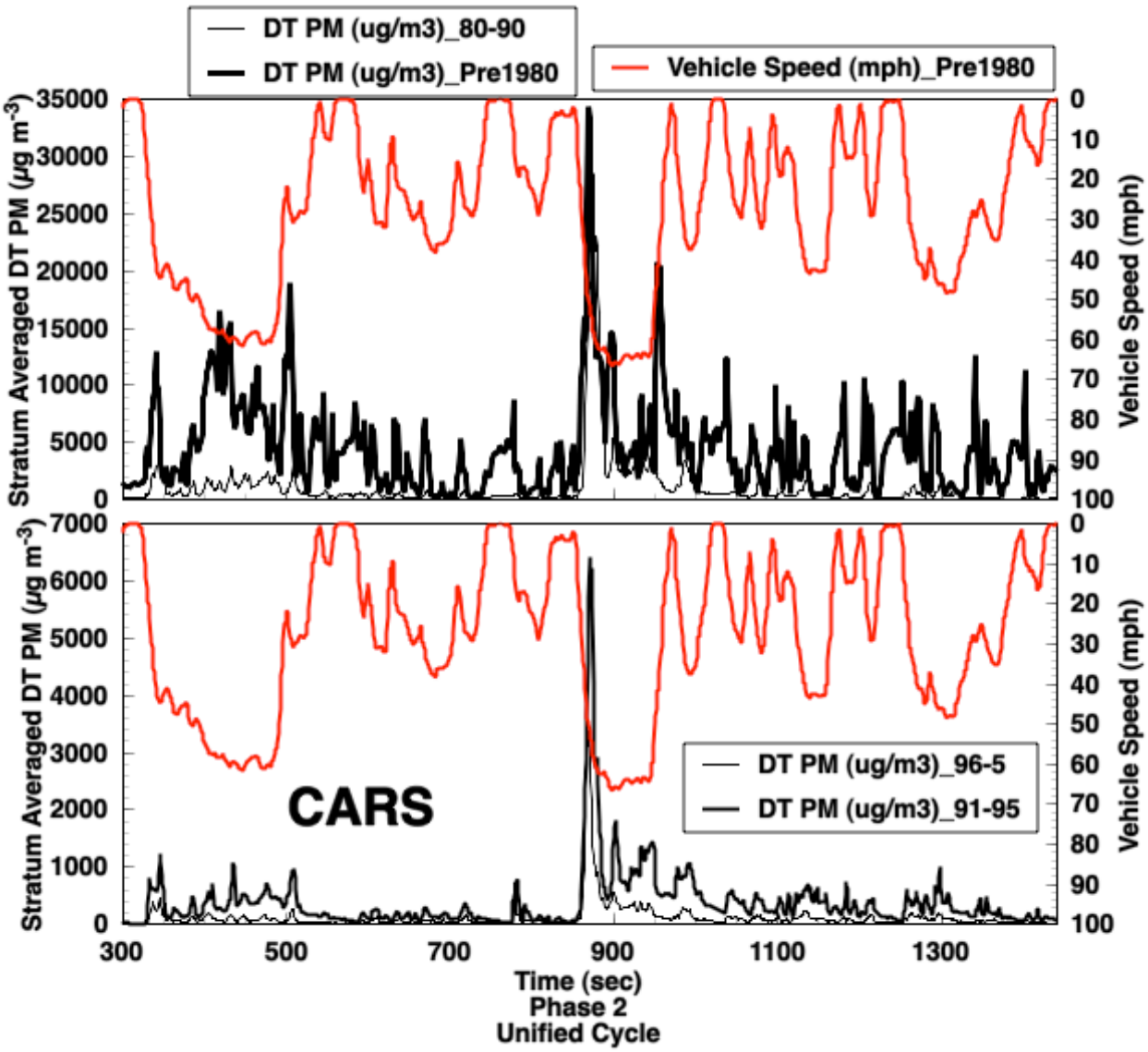

Figure 14. DustTrak PM emissions during phase 2 of the unified cycle for newer (lower graph) and older (upper graph) vehicles. Note that PM emissions peak during the aggressive acceleration in about the middle portion of the cycle right before 900 seconds. Note in the upper graph that the oldest category of vehicles had high emission on both accelerations as well as decelerations. Note that the older vehicles shown in the upper graph had about a factor of 5 more emission during the high acceleration portion of the cycle before 900 seconds.

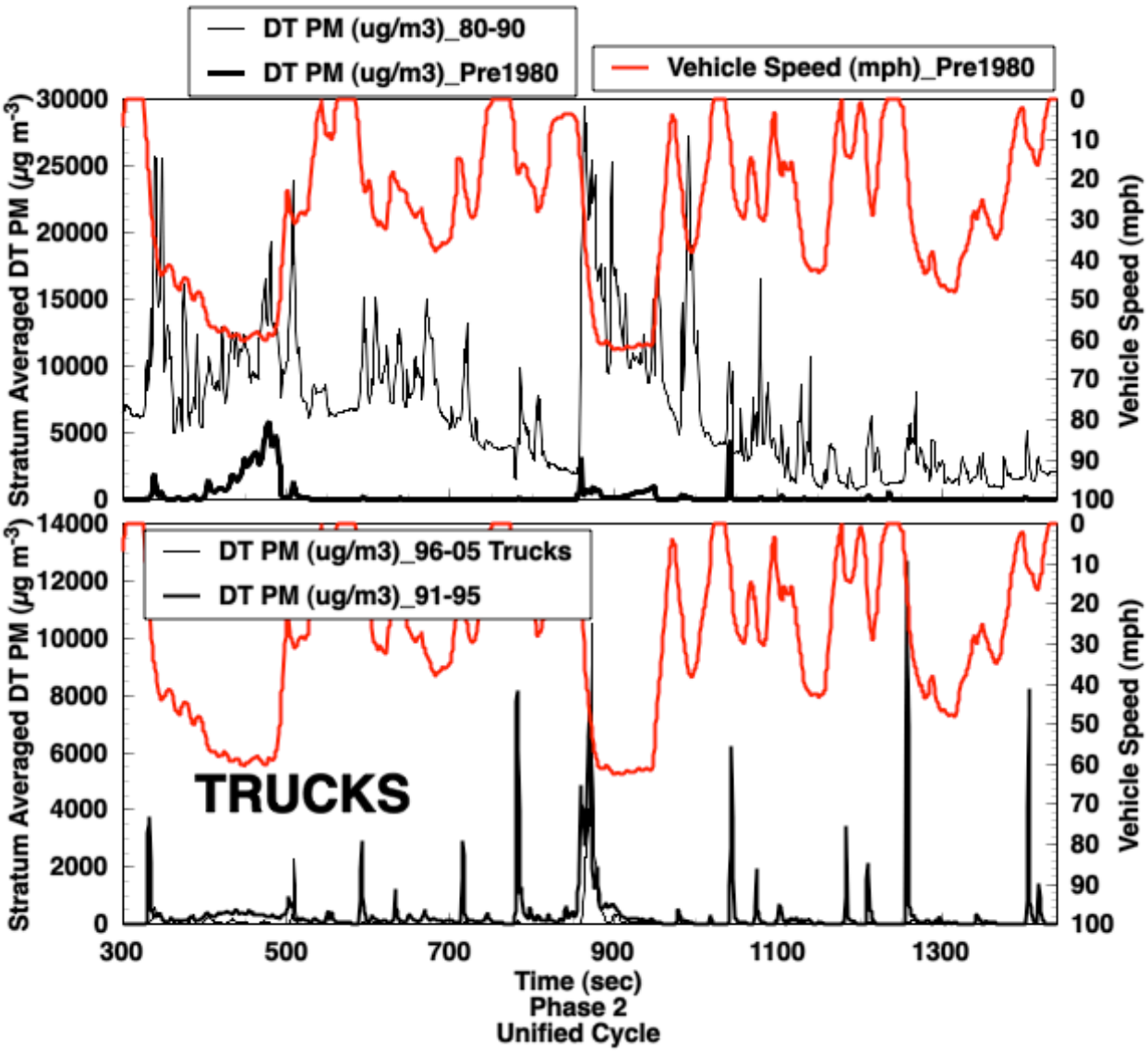

Figure 15. Same as Figure 14, though for trucks instead of passenger cars. Newer cars (see the lower graph in Fig. 14) have about 1/2 the emissions as newer trucks (lower graph above) and both have peaks during accelerations.

Table 1. Emission rates in mg/mile for phase 1 of the unified cycle for cars and trucks.

PHASE 1	Year	BC car	DT PM car	DR PM car	BC Truck	DT PM Truck	DR PM Truck
	1970-1980	63.89	249.17	396.67	72.45	171.48	194.18
	1981-1990	18.09	112.66	781.77	19.66	324.84	4557.90
	1991-1995	4.38	26.09	73.35	3.41	33.10	171.11
	1996-2005	3.58	27.19	167.46	4.08	14.90	14.04

Table 2. Emission rates in mg/mile for phase 2 of the unified cycle for cars and trucks.

PHASE 2	Year	BC car	DT PM car	DR PM car	BC Truck	DT PM Truck	DR PM Truck
	1970-1980	25.45	138.36	677.82	0.87	9.23	69.60
	1981-1990	4.89	33.15	213.71	4.78	214.16	3800.55
	1991-1995	0.74	11.83	70.61	0.53	10.93	78.37
	1996-2005	0.30	3.77	31.99	0.50	3.16	2.78

Table 3. Emission rates in mg/mile for phase 3 of the unified cycle for cars and trucks.

PHASE 3	Year	BC car	DT PM car	DR PM car	BC Truck	DT PM Truck	DR PM Truck
	1970-1980	37.50	92.12	105.60	1.92	4.81	4.69
	1981-1990	3.84	22.19	142.74	7.26	192.03	2086.77
	1991-1995	0.77	7.16	13.27	0.78	18.85	78.67
	1996-2005	0.25	2.25	3.75	0.43	1.82	2.14

Emission rates for each phase of the unified cycle, for each stratum of vehicles model year ranges, for black carbon (BC) and total particle mass (PM) are given in Tables 1 through 3. PM obtained from the DustTrak nephelometer are indicated by "DT" and those from the DataRAM4 are given by "DR". Note that BC emission rates generally decrease from older to newer vehicles, though because the class of older trucks (pre 1980) was only represented by 2 vehicles the statistics are thin here. Note that BC and DT PM emission rates were highest (for cars) during phase 1, though phase 2 and 3 values were similar. Note that emission rates computed from the DataRAM4 (DR) are usually way in excess of those obtained with the DustTrak, except for those cases of low emission rates. The DataRam4 seems to have a problem

with high concentrations where it seems some optics gets dirty, and this adds scattering amount that gets interpreted erroneously as PM.

Note the interesting truck values for the 1970-1980 stratum. The BC emission rates were very high for this category in phase 1, though were much lower once the vehicles warmed up in phases 2 and 3. These emission rates were computed from the nominal miles driven, on the average, during each phase, and from the nominal sample volume pulled through the constant volume sampler. The uncertainty introduced by using nominal values is likely around 20%. Phase 1, 2, and 3 miles driven were taken to be 1.18 miles, 8.6 miles, and 1.18 miles. The flow volume was 71.75 m^3 for phases 1 and 3, and 267.8 m^3 for phase 2.

REFERENCES

Anderson, T. L. and J. A. Ogren (1998). "Determining Aerosol Radiative Properties Using the TSI 3563 Integrating Nephelometer." Aerosol Science and Technology **29**(1): 57-69.

Arnott, W. P., H. Moosmueller and J. W. Walker (2003). Photoacoustic instrument for measuring particles in a gas. USA Patent 6,662,627, Desert Research Institute, Reno NV.

Arnott, W. P., H. Moosmüller, C. F. Rogers, T. Jin and R. Bruch (1999). "Photoacoustic spectrometer for measuring light absorption by aerosols: Instrument description." Atmospheric Environment **33**: 2845-2852.

Arnott, W. P., H. Moosmüller and J. W. Walker (2000). "Nitrogen dioxide and kerosene-flame soot calibration of photoacoustic instruments for measurement of light absorption by aerosols." Review of Scientific Instruments **71**(7): 4545-4552.

Arnott, W. P., B. Zielinska, C. F. Rogers, J. Sagebiel, K. E. Kelly, D. A. Wagner, A. F. Sarofim and J. S. Lighty (2004). "Evaluation of 1047 nm photoacoustic instruments and photoelectric aerosol sensors in source-sampling of black carbon aerosol and particle bound PAH's from gasoline and diesel powered vehicles." Environmental Science and Technology **submitted 15 March**.

Chow, J., J. Watson, D. Crow, D. Lowenthal and T. Merrifield (2001). "Comparison of IMPROVE and NIOSH Carbon Measurements." Aerosol Science and Technology **34**(1): 23-34.

Chow, J. C., J. G. Watson, L. C. Pritchett, W. R. Pierson, C. A. Frazier and R. G. Purcell (1993). "The DRI thermal/optical reflectance carbon analysis system: Description, evaluation and applications in U.S. air quality studies." Atmospheric Environment **27A**: 1185-1201.

Dalzell, W. H. and A. F. Sarofim (1969). "Optical constants of soot and their application to heat flux calculations." Journal of Heat Transfer: 100-104.

Fuller, K. A., W. C. Malm and S. M. Kreidenweis (1999). "Effects of mixing on extinction by carbonaceous particles." Journal of geophysical research **104**(D13): 15941-15954.

Japar, S. M. and D. K. Killinger (1979). "Photoacoustic and absorption spectrum of airborne carbon particulate using a tunable dye laser." Chemical Physics Letters **66**: 207-209.

Japar, S. M. and A. C. Szkarlat (1981). "Measurement of Diesel Vehicle Exhaust Particulate Using Photoacoustic Spectroscopy." Combustion Science and Technology **24**: 215-219.

Japar, S. M. and A. C. Szkarlat (1981). Real-time measurements of diesel vehicle exhaust particulate using photoacoustic spectroscopy and total light extinction. Fuels and Lubricants Meeting, Tulsa OK, SAE.

Japar, S. M., A. C. Szkarlat and W. R. Pierson (1984). "The determination of the optical properties of airborne particle emissions from diesel vehicles." The Science of the Total Environment **36**: 121-130.

Moosmüller, H., W. P. Arnott, C. F. Rogers, J. L. Bowen, J. A. Gilles, W. R. Pierson, J. F. Collins, T. D. Durbin and J. M. Norbeck (2001). "Time resolved characterization of diesel particulate emissions. 1. Instruments for particle mass measurements." Environmental science & technology **35**(4): 781-787.

Moosmüller, H., W. P. Arnott, C. F. Rogers, J. L. Bowen, J. A. Gillies, W. R. Pierson, J. F. Collins, T. D. Durbin and J. M. Norbeck (2001). "Time resolved characterization of particulate emission: 2. Instruments for elemental and organic carbon measurements." Environmental Science & technology **35**: 1935-1942.

Petzold, A. and R. Niessner (1994). The Photoacoustic Soot Sensor for Black Carbon Monitoring. Fifth International Conference on Carbonaceous Particles in the Atmosphere, Berkeley, CA.

Petzold, A. and R. Niessner (1995). "Novel Design of a Resonant Photoacoustic Spectrophone for Elemental Carbon Mass Monitoring." Applied Physics Letters **66**(10): 1285-1287.

Roessler, D. M. (1984). "Photoacoustic Insights on Diesel Exhaust Particles." Applied Optics **23**(8): 1148-1155.

Sioutas, C., S. Kim, M. Chang, L. L. Terrell and H. Gong (2000). "Fied evaluation of a modified DataRAM MIE scattering monitor for real-time PM2.5 mass concentration measurements." Atmospheric Environment **34**: 4829-4838.

Terhune, R. W. and J. E. Anderson (1977). "Spectrophone Measurements of the Absorption of Visible Light by Aerosols in the Atmosphere." Optics Letters **1**(2): 70-72.

Watson, J. G., J. C. Chow, D. H. Lowenthal and L. C. Pritchett (1994). "Differences in the carbon composition of source profiles for diesel- and gasoline-powered vehicles." Atmospheric environment **28**(15): 2493-2505.